Monte Carlo simulations of the thermodynamic behavior of exchange graded ferromagnets

J. S. Salcedo-Gallo,[1,*] L. Fallarino,[2] J. D. Alzate-Cardona,[1] E. Restrepo-Parra,[1] and A. Berger[2]
[1]*Departamento de Física y Química, Universidad Nacional de Colombia, Manizales, Colombia*
[2]*CIC nanoGUNE BRTA, E-20018 Donostia - San Sebastián, Spain*

(Received 25 October 2020; accepted 6 March 2021; published 25 March 2021)

In this work, we investigate the thermodynamic behavior of exchange graded ferromagnetic films using Monte Carlo simulations. The systems are modeled by using a classical Heisenberg Hamiltonian, considering only nearest neighbor exchange interactions and a linear depth-dependent effective magnetic exchange coupling strength profile. Our quantitative assessment of the local physical quantities shows that each layer exhibits rather isolated thermodynamic behavior, since both layerwise magnetization and susceptibility data indicate layer-specific "local" Curie temperatures as a consequence of the depth-dependent change in the exchange coupling strength. We also propose and evaluate a predictive formulation for such profiles of "local" Curie temperatures, whose only input is the pre-selected exchange coupling profile. Having this very precise predictive tool, we show how it can be used to obtain the temperature-dependent ferromagnetic state including its depth-dependent magnetization profile at any given temperature. Thus, it is possible to predict which exchange profile will produce a desired thermodynamic behavior and associated functionality, without the need to perform complex experiments or time-consuming computations. With this study, we furthermore demonstrate that nonlocal aspects of the thermodynamic state formation in graded magnetic materials are relevant only over very short length scales, which is in outstanding qualitative agreement with prior numerical and experimental work.

DOI: 10.1103/PhysRevB.103.094440

I. INTRODUCTION

In the past few decades, the understanding of magnetic properties of multilayer structures had led to very significant advances in materials research. For instance, starting in the early 1990s, exchange spring ferromagnets were established as an interesting and successful approach for materials design [1]. The first studied exchange spring ferromagnet consisted hereby of two exchange-coupled ferromagnetic layers, of which one exhibited high magnetic anisotropy and low magnetic moment, while the other had low magnetic anisotropy and high magnetic moment [1]. The coupled bilayer configuration led to an enhanced energy product if compared to the values of the constituting layers [1–3]. The theoretical description and further experimental realization of exchange spring magnets provided a convenient model system for developing precise spatial control of the magnetic properties in multilayer systems, given that the relative thicknesses of the hard- and soft-magnetic layers could be controlled during the deposition process [2–7]. Such spatial control has later opened intriguing possibilities for improving magnetic recording technologies [8–10].

Following this multilayer stacking approach, anisotropy graded materials were proposed and experimentally realized, driven by theoretical predictions that they should exhibit even better performance [11–15]. Hereby, it was found that a depth-dependent gradient of the magnetic anisotropy constant (K) could be realized either by controllably tuning the thickness of the constituent layers or via heat treatment during deposition [11–15]. However, these materials did not achieve significant technological relevance because of their fabrication complexity and their rather modest performance gains. Nevertheless, the successful achievement of vertically graded anisotropy profiles provided remarkable insights towards unveiling novel functionalities associated with the spatial control of the modified energetic terms in such systems.

More recent studies have demonstrated that not only K gradients can be achieved and tailored, but that it is also possible to achieve continuous gradients in the exchange coupling constant (J) along the growth direction in compositionally graded layer systems [16–18]. Hereby, it is important to point out that from a thermodynamic point of view, ferromagnetic (FM) materials undergo a second-order phase transition at a single temperature, the Curie temperature (T_c), which can be tuned by alloying a FM material with a "nonmagnetic" material [18–21]. In such alloys, a reduction in T_c is typically related to an increase of the "nonmagnetic" material in the alloy composition. However, in conventional itinerant ferromagnets the resulting ferromagnetism is associated with a collective electronic state that is more complicated than a mere combination of exchange coupled and uncoupled atoms, in which the nonmagnetic atoms would be represented in a simplistic fashion as nonexistent voids from a magnetic perspective [22–25]. Therefore, it is actually more sensible to represent a graded material via a depth dependent J profile rather than by different local exchange coupling constants representing individual atoms of different kinds, because this better reflects the average local composition impact onto the ferromagnetic

*jussalcedoga@unal.edu.co

exchange, which is associated with composition gradients in such alloys [18–21].

Recent studies have now shown that such materials actually behave as if they were composed of virtually independent ferromagnetic segments as far as their thermodynamic phase is concerned, so that each local J value generates behavior consistent with a "local" Curie temperature ($\tilde{T}_c$) [18–21]. This type of sample behavior allows one to map the temperature-dependent ferromagnetic state onto a depth-dependent spatial profile, as first confirmed both experimentally and theoretically in Ref. [18]. It was demonstrated that as a consequence of the spatial nature of the ferromagnetic state, a quasi phase-boundary emerges that separates ordered from disordered magnetic regions within the same ferromagnetic sample, which can be altered controllably and reversibly by temperature and/or magnetic field [20]. Recent studies have explored this functionality even in epitaxially grown samples, featuring precisely engineered J profiles within a single crystal material [18–21]. Due to the epitaxial nature of these samples, it is then possible to achieve a well-defined in-plane easy axis, so that their general magnetic behavior is very simple, and the depth-dependent J-profile induced properties and their impact onto the temperature dependent magnetization profile can be very easily observed [19,26].

Most relevantly, these previous studies have demonstrated that the thermodynamic state of the magnetization is dominated by the local exchange coupling strength only and that collective effects can be suppressed all the way down to a length scale of about 2 nm or even less [18–21]. Such a high degree of localization is counterintuitive if one considers that ferromagnetism is a collective phenomenon and that the studied systems furthermore utilized metallic band ferromagnets with delocalized spin-polarized states [20]. This thermodynamic property isolation represents a very relevant result, given that the observed spatial localization limit lies within the realm of nanotechnology applications today, such as hard disk drive media structures [19,20]. Furthermore, it has been demonstrated that temperature-controlled interlayer exchange coupling in strong/weak ferromagnetic multilayers can lead to tunable collective magnetization reversal that could be utilized in novel devices based on thermally assisted switching [27–29]. So, while the experimental work has been very successful and seen substantial progress in the last few years, theoretical efforts were lacking and have been limited to mean-field type calculations only so far [18,21]. However, it is important to mention that there are other important techniques for studying many-body physics problems, which can be extended to the study of exchange graded materials, such as the constant coupling approximation [30], cluster methods [31], Green's function theory [32–34], random-phase and parametric approximations [35,36], and renormalization group theory [37], for instance. Specifically, previous works had studied the problem of calculating Curie temperatures for layered structures, in which the (Heisenberg) intra- and interlayer exchange interactions were allowed to differ, paying particular attention to weakly interacting layer systems [32]. Moreover, a renormalization group theory approach on the critical thermodynamics of inhomogeneous ferromagnetic systems predicted, under specific conditions, an emerging "local" critical behavior and thus a "local" critical temperature in the studied system [37].

In this work, we explore Monte Carlo (MC) simulations of exchange graded materials, given the superiority of this computational method to provide accurate calculations and relevant insights into the underlying physical effects governing the macroscopic ferromagnetic state in nanoscale materials [38,39]. Specifically, we aim to explore whether the experimentally observed localized behavior can be corroborated by considering a nearest neighbor classical Heisenberg model with a linear depth-dependent effective exchange coupling strength profile to mimic the systematic compositional changes in experimental samples. We also consider it worthwhile to study whether it might be feasible to derive a general predictive description of local magnetization states from our MC simulation results. This would enable anyone to make accurate predictions of temperature dependent magnetization profiles based upon the exchange coupling strength J profiles alone, without having to rely upon complex and time-consuming computations or experiments.

This paper is organized as follows: In Sec. II, we describe details regarding the utilized model and the method that we used to perform our simulations. In Sec. III A, we present a qualitative agreement in between simulations and available experimental data for the nanoscale modulated film structure that was reported in Ref. [21]. In Sec. III B, we demonstrate based upon our simulated data that a local $\tilde{T}_c$ and its profile is a meaningful way to characterize the thermodynamic behavior of graded samples. Furthermore, in Sec. III C, we explore the effect of specific exchange profiles and gradient values onto local magnetic properties. Section III D is devoted to the development of an accurate predictive description of local magnetic properties for exchange graded materials. In Sec. IV, we summarize our work, provide conclusions, and give a further outlook. Lastly, we include an Appendix to address the finite-size effects in our simulations.

II. MODEL AND METHOD

In this work, we studied the thermodynamic behavior of exchange graded samples by means of MC simulations. We based our computations on samples exhibiting a fcc crystal structure and a (111) surface orientation, whose schematic representation is shown in the inset of Fig. 1. This specific choice is based on the fact that we were aiming to compare our results with prior computational and experimental findings, and thus, we chose the crystal structure studied in Ref. [18]. It is important to mention that our simulations are based on a three-dimensional system that has a one-dimensional gradient along the vertical direction to ensure that the finite size of the simulated samples would not interfere with the gradient itself.

Furthermore, the simple geometry employed in this work will make the analysis straightforward and shall make it possible to check the extent and limits of localization of thermodynamic behavior in graded ferromagnetic materials. Despite the fact that we consider only nearest neighbors to be exchange coupled, we obtain a strong interlayer exchange coupling for the utilized geometry, namely half of the total exchange field originates from interlayer coupling, given that

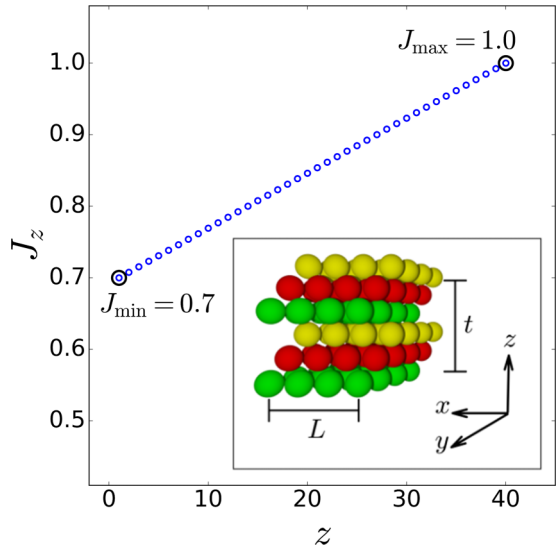

FIG. 1. Intralayer exchange coupling J_z as a function of depth z, which is the geometry investigated in this work. Specifically, we are displaying here a gradual 30% reduction in the exchange strength along the z direction, with respect to $J_{max} = 1.0$. Inset: schematic of the fcc (111) lattice investigated here, shown for the specific case of $L = 4$ and $t = 6$, with L being the lateral dimension and t the total thickness of the sample in units of the number of layers. Periodic boundary conditions (PBC) were applied in the x-y plane, whereas free boundary conditions (FBC) were imposed along the z axis to mimic surface effects.

6 of the 12 nearest neighbors are located in adjacent layers. Thus, one would intuitively not expect that the thermodynamic properties of such materials were strongly localized, even if our approach of including only nearest neighbor exchange coupling is rather simplistic and not a fully realistic description of graded materials. Despite this simplification, local spin models have been successfully utilized in the past for the computation of thermodynamic properties of confined itinerant ferromagnets [22,24,38]. So, our approach seems sensible despite its overall simplified assumptions.

As it has been asserted in previous studies, continuous and controlled variations in composition can be utilized to induce continuous changes in J [18–21]. To model and investigate this here, we consider a linear-gradient exchange coupling profile, with the effective intralayer exchange strength J_z between a spin and its nearest neighbors in the same layer given by

$$J_z = \frac{(J_{max} - J_{min})}{t - 1}(z - 1) + J_{min}, \tag{1}$$

where t is the thickness of the sample in units of atomic layers (z) so that $1 \leqslant z \leqslant t$. For simplicity, but without impacting the general validity of our approach, we choose $J_{max} = 1.0$ so that J_{min} corresponds to the ratio of the lowest to highest T_c of two uniform reference samples, representing the exchange coupling strength on either side of our graded film. Thence, $J_{max} - J_{min}$ determines the absolute reduction in the exchange strength along the vertical dimension, whereas the gradient $dJ_z/dz = (J_{max} - J_{min})/(t - 1)$ determines the rate at which J_z varies along the z axis, whose units are defined as the J_z reduction (in percent of J_{max}) per layer. Thus, our geometry closely follows the linear-gradient exchange profile achieved in Ref. [18].

Figure 1 shows the linear-gradient J_z profile obtained with Eq. (1), featuring a gradual 30% reduction in the exchange strength along the z direction, using J_{max} as the base value. The black circles denote J_{min} and J_{max} as the J_z values at the surface layers of the graded sample, which also define the J values for the two uniform reference samples that we have computed. The interlayer exchange coupling strength $[J_{z(z+1)}]$ between a spin and its nearest neighbors in the neighboring plane is considered to be the arithmetic average between J_z and $J_{(z+1)}$, so that $J_{z(z+1)} = (J_z + J_{(z+1)})/2$. The specific atoms positions for the different constituting alloy materials and atom type dependent exchange coupling constants are not explicitly considered here. Therefore, Eq. (1), and the further resulting interlayer coupling constants, can be understood as representing an effective exchange coupling that is adequate for each layer's averaged alloy concentration, and thus, rudimentary mimics itinerant exchange coupling aspects within our local spin model. In our simulations, we included periodic boundary conditions (PBC) in the x-y plane to approach translational invariance within the plane of each layer, whereas free boundary conditions (FBC) were imposed along the z axis in order to mimic surface effects on an actual thin film. In the inset of Fig. 1, it can be seen that L determines the system size in the x-y plane in a quadratic manner, and any spurious finite-size effects should be related to this quantity. We have explicitly verified the influence of L, which is described in the Appendix, where we observe conventional finite size scaling for the simulated graded samples. More importantly, the boundary conditions imposed in our computations are intended to mimic the actual physical system, where the thickness is far smaller than the lateral dimensions, resulting in negligible in-plane demagnetization fields [19,20].

The magnetic behavior of the system was modeled using a classical Heisenberg Hamiltonian that is considered to be a mere superposition of layer-wise terms, including only exchange interactions between a spin and its nearest neighbors in the same layer and its neighboring layers, as given by Eq. (2).

$$\mathcal{H} = -\sum_{z=1}^{t}\left(\sum_{\langle i,j\rangle} J_z(\boldsymbol{S}_i \cdot \boldsymbol{S}_j) + \sum_{\langle i,k\rangle} J_{z(z+1)}(\boldsymbol{S}_i \cdot \boldsymbol{S}_k)\right) \tag{2}$$

where $\boldsymbol{S}_i$, $\boldsymbol{S}_j$, and $\boldsymbol{S}_k$ are the spins of the magnetic sites labeled i, j, k with $|\boldsymbol{S}_i| = |\boldsymbol{S}_j| = |\boldsymbol{S}_k| = 1.0$. The i, j, k indices mean that the summations are taken to account for the interactions of spin i with its j and k nearest neighbors in the same and adjacent atomic plane. Please note that the first and second terms in the first summation of Eq. (2) correspond to the intra- and interlayer exchange interactions, respectively. However, one should not add the interlayer exchange interactions for the last layer because there is no layer $t + 1$, and thus $J_{t(t+1)} = 0$.

For simplicity, we have neglected anisotropy and Zeeman energy terms in our MC simulations, given that exchange interactions are dominant in conventional ferromagnets [38]. However, it is important to point out that the spin (size) that we are using here is independent from the layer, which turns out to be a sensible assumption to study the effect of the exchange profile only. Albeit, this is actually not the same in

experiments, because, when varying the alloy, it is not just J or T_c that changes, but also the local saturation magnetization (M_s), as it has been observed experimentally in Ref. [26] for uniform CoRu-alloy films with different Ru concentrations. Although we are not considering this particular aspect here, it is worthwhile mentioning that, if an external field would have been applied, the experimental M_s effect would have been very relevant indeed, and one would have to consider a layer-wise magnetic moment to characterize the influence of the Zeeman term onto the thermodynamic behavior of graded materials correctly. Moreover, we are primarily interested in characterizing the expansion of the ferromagnetic state in the presence of an already existing and thus stabilizing ferromagnetic entity, namely the initially ordered film segment. As such, we can ignore formal problems that are related to the lack of spontaneous symmetry breaking for $T > 0$ in two-dimensional systems in the absence of anisotropy or dipolar interactions that result from the Mermin-Wagner theorem [40,41]. In practice, the finite size of our simulations produces an energy gap in the spin wave spectrum that leads to a stabilization of the ferromagnetic state.

The simulations presented in this work were carried out using VEGAS [42], which is an open-source package for the atomistic simulation of magnetic materials, using the MC method based on the Metropolis algorithm. Furthermore, we used an adaptive spin update policy for an optimal phase space sampling of Heisenberg spin systems [43]. Simulations were performed with temperatures ranging from $k_BT/J_{\max} = 4.5$ down to $k_BT/J_{\max} = 0.5$. In addition, we executed $N \times N_{\mathrm{MCS}}$ Monte Carlo steps (MCS) for every temperature, rejecting the first half of all MCS for relaxation, with $N_{\mathrm{MCS}} = 2\times10^4$ and $N = L\times L\times t$ being the total number of spins within the sample. To compute statistical errors in the temperature-dependent physical observables, we simulated five different initializations per configuration, for every temperature and every system explored in this work.

The volume averaged temperature-dependent magnetization was computed as

$$\frac{M}{M_s} = \frac{1}{N}\left|\sum_i^N \boldsymbol{S}_i\right|. \tag{3}$$

In addition, the layer-wise temperature-dependent magnetization was computed as

$$\frac{M(z)}{M_s} = \frac{1}{N_z}\left|\sum_{i\in z}^{N_z} \boldsymbol{S}_i\right|, \tag{4}$$

where N_z corresponds to the number of spins in each layer, i.e., $N_z = L\times L$.[1] Furthermore, by using the fluctuation-dissipation theorem [46], we can compute the temperature-dependent susceptibility, using

$$\frac{\chi}{M_s^2} = \frac{\langle M^2\rangle - \langle M\rangle^2}{k_BT}. \tag{5}$$

Analogously, the layer-wise temperature-dependent susceptibility was computed as

$$\frac{\chi(z)}{M_s^2} = \frac{\langle M(z)^2\rangle - \langle M(z)\rangle^2}{k_BT}. \tag{6}$$

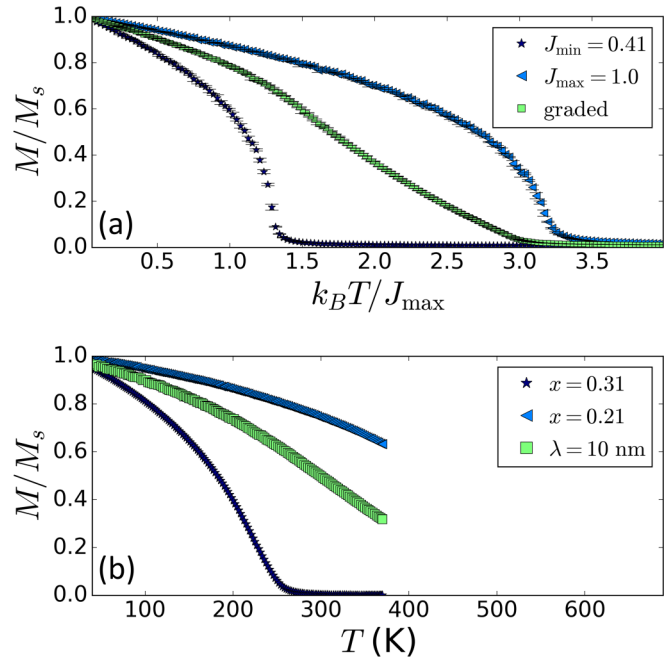

FIG. 2. Temperature-dependent magnetization curves for graded and uniform systems. (a) Simulated by means of the MC method for two uniform reference samples with $J_{\min}$ and $J_{\max}$, respectively, and a sample featuring a single-gradient magnetic exchange profile exhibiting a 59% absolute reduction in the exchange strength along the z direction, using $J_{\max} = 1.0$ as a base. (b) Adaptation of the data reported in Ref. [21], for two uniform epitaxial $Co_{1-x}Ru_x$ thin films with $x = 0.21$ and $x = 0.31$, and another sample featuring a nanometer-scale triangular wavelike concentration depth profile of the same alloy. The modulated sample was engineered to have a nominal modulation period of $\lambda = 10$ nm.

III. RESULTS AND DISCUSSION

A. Qualitative behavior

Figure 2(a) shows simulated $M(T)$ data for a sample featuring the linear-gradient J_z profile of Eq. (1), with $t = 60$ and $J_{\max} - J_{\min} = 0.59$ (green squares). In this case, the chosen value of $J_{\min} = 0.41$ corresponds to the ratio of the lowest to highest Curie temperatures of two epitaxial $Co_{1-x}Ru_x$ reference samples studied in Ref. [21]. This figure also shows the simulated $M(T)$ data for the two uniform reference samples with $J_{\min}$ and $J_{\max}$, respectively (blue stars and triangles). These reference samples exhibit conventional ferromagnetic phase transitions, following a typical power-law type behavior, with the uniform sample with $J_{\max}$ having a larger T_c than the uniform sample with $J_{\min}$, whereas the curve of the graded sample falls in between and exhibits a more gradual

[1] As usual in MC simulations, the usage of $|M|$ instead of M in Eqs. (3) and (4) is related to the finite size of the simulated system, for which magnetization reversal can occur occasionally, while it should not occur in the thermodynamic limit [44]. As such, $|M|$ is used in our simulations to mimic the thermodynamic limit and avoid the impact of finite activation barriers, which therefore stabilizes the ferromagnetic state for $k_BT/J > 0$ [45].

$M(T)$ dependency. Such behavior is indicative of the fact that the net magnetization of the graded sample can be considered as a superposition of nearly independent curves with distinct $\tilde{T}_c$ [18–21]. This behavior reflects the fact that the ferromagnetically ordered fraction of the film shrinks in volume with increasing temperature [18], which results from the temperature-controlled displacement of an emergent quasi phase-boundary separating ordered from disordered magnetic regions within the sample [18–21]. Moreover, Fig. 2(a) shows that the global T_c of the graded sample is not the same as the T_c of the uniform reference sample with $J_{\max}$. This difference in T_c is found to be non-negligible and will be analyzed in detail later.

The data points presented in Fig. 2(b) are an adaptation of those reported in Fig. 2 of Ref. [21]. This figure shows the experimental $M(T)$ data for a compositionally modulated $Co_{1-x(z)}Ru_{x(z)}$ film (green squares), featuring a symmetric triangular concentration depth profile, with a modulation period of $\lambda = 10$ nm between $x = 0.21$ to $x = 0.31$. This figure also shows the experimentally obtained $M(T)$ data for uniform $Co_{1-x}Ru_x$ reference samples with $x = 0.31$ and $x = 0.21$ (blue stars and triangles), which exhibit both low ($T_c = 230$ K) and high ($T_c = 560$ K) ferromagnetic phase transition temperatures. It is worth mentioning that all these experimental samples were epitaxially grown, exhibiting an hcp crystal structure and a $(10\bar{1}0)$ surface orientation, so that they exhibit a uniaxial in-plane easy axis, along which the experimental $M(T)$ data were measured. It can be seen from Fig. 2(b) that the reference sample with the highest Ru concentration, $x = 0.31$ (blue stars), exhibits a much lower T_c than does the $x = 0.21$ sample (blue triangles), whereas the graded curve (green squares) smoothly falls in between. Therefore, and as previously indicated, this behavior is compatible with being a mere superposition of distinct curves, corresponding to virtually independent ferromagnetic segments within the sample [18–21]. Such a smoothly varying $M(T)$ curve for the modulated sample turns out to be very similar to what would be expected from the $M(T)$ behavior of a superposition of independent alloy samples covering the total concentration range [21]. It should be mentioned that the measurement temperatures in Ref. [21] were restricted to $T < 370$ K to avoid sample damage. Overall, Figs. 2(a) and 2(b) show an outstanding qualitative agreement, which corroborates that our model works despite its inherent simplifying assumptions.

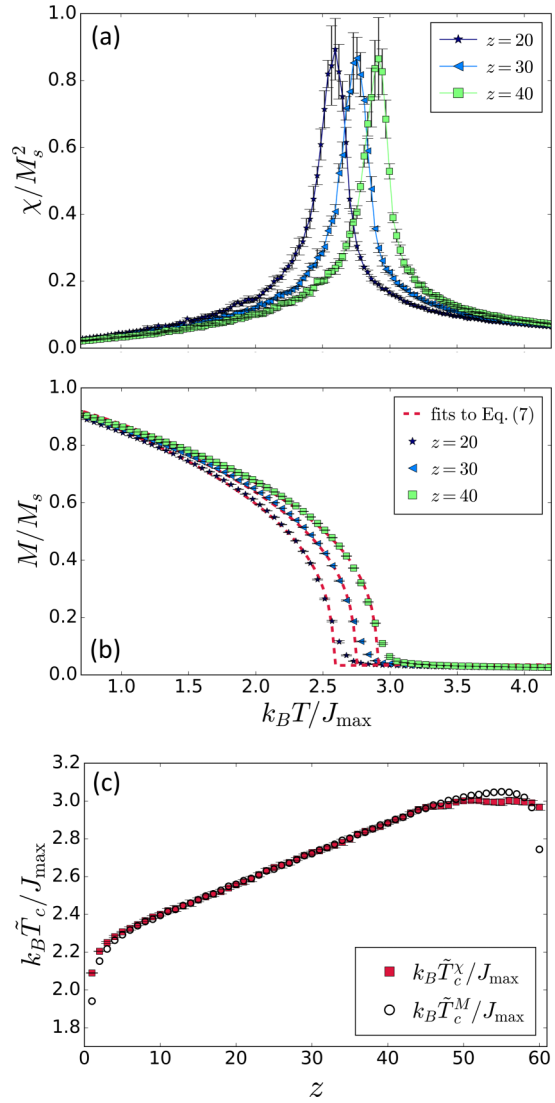

FIG. 3. (a) Temperature-dependent susceptibility curves, which we utilized to estimate $\tilde{T}_c^{\chi}$, for some selected inner layers ($z = 20, 30, 40$) of a graded sample exhibiting $J_{\max} - J_{\min} = 0.3$ and $t = 60$. (b) Temperature-dependent magnetization curves for the same selected inner layers shown in (a). The red dashed lines in (b) correspond to fits to the Kuz'min functional form [Eq. (7)] with $s = 1.757$ and $p = 5/2$, which we used to estimate $\tilde{T}_c^{M}$. (c) Comparison between the two $\tilde{T}_c$ estimates: $\tilde{T}_c^{\chi}$ and $\tilde{T}_c^{M}$ as a function of z.

B. Quantitative assessment of the "local physical observables" in exchange graded materials

Prior studies using experiments and mean-field calculations have shown that graded materials behave very similar to a mere superposition of independent ferromagnetic segments, as far as their thermodynamic magnetization state is concerned [18,21]. Correspondingly, we investigated this particular aspect by means of MC simulations, which are more accurate than mean-field computations and generally not prone to false predictions such as two-dimensional ferromagnetism in Heisenberg model systems, for instance [47–49]. For this purpose, we used a sample featuring the single-gradient J_z profile of Eq. (1), with $t = 60$ and $J_{\min} = 0.7$, thus recreating a 30% absolute reduction in the exchange strength along z, with respect to $J_{\max} = 1.0$. In the following, $J_{\min} = 0.7$ is generally utilized to mimic experimental observations and mean-field calculations of Ref. [18]. However, there is nothing unique about those values and our findings here are generally applicable.

Figure 3(a) shows computed layer-specific susceptibility vs. T dependencies according to Eq. (6) for some selected inner layers of a $t = 60$ graded sample, in particular $z = 20$, 30, and 40. We observe that the curves for individual layers all exhibit a sharp peak that is indicative of a phase transition at the peak position temperature, and we see that the temperatures at which the peaks occur change with z. Specifically, for larger z values, corresponding to higher J_z, the perceived transition temperature $\tilde{T}_c$ increases as well. Notably, the $\chi(z)$

peaks show approximately the same height and width regardless of z, which therefore suggests that the system evolves in a highly localized fashion and that neighboring layers do not considerably influence the temperature-driven fluctuations of the local $M(z)$ data at different z values.

Other evidence of the localized behavior is presented in Fig. 3(b), which shows local $M(z)$ data for the same selected layers of Fig. 3(a). Figure 3(b) shows that individual inner layers of the graded sample exhibit the typical behavior of the order parameter in ferromagnetic materials, displaying an apparent power-law type of behavior, with each curve pointing to very different local ordering temperatures $\tilde{T}_c$ at which the magnetization approaches zero. Furthermore, it can be seen that as z increases, $\tilde{T}_c$ increases as well, following the same corresponding behavior depicted in Fig. 3(a). To analyze the data quantitatively and specifically to extract the local ordering temperature $\tilde{T}_c$, we have fitted our simulation results with the functional form described by Kuz'min

$$\frac{M(z)}{M_s} = \begin{cases} \left[1 - s\left(\frac{T}{\tilde{T}_c^M}\right)^{3/2} - (1-s)\left(\frac{T}{\tilde{T}_c^M}\right)^{p}\right]^{1/3} & \text{for} \quad T/\tilde{T}_c^M \leqslant 1 \\ k & \text{for} \quad T/\tilde{T}_c^M > 1 \end{cases}, \tag{7}$$

where $p = 5/2$ for most ferromagnets [50], while s, $\tilde{T}_c^M$, and k are fitting parameters. In contrast to Kuz'min's original formulation, we added k as the magnetization offset for $T > \tilde{T}_c^M$ because our simulations exhibit a spurious "paramagnetic magnetization", which is associated with the finite size of the lateral dimensions in our simulations (see Appendix). The red dashed lines in Fig. 3(b) show the individual fits to the local $M(z)$ curves using Eq. (7),[2] which demonstrates that Eq. (7) is very well suited to describe the individual temperature-dependent magnetization curves for a wide range of the simulated temperatures. The fits only produce very minor deviations in the immediate vicinity of $\tilde{T}_c$, which is a general MC simulation issue given the inherent rounding of critical properties due to finite-size effects [51].

Overall, both Figs. 3(a) and 3(b) clearly indicate "local thermodynamic behavior," and therefore validate and substantiate the concept of having a local $\tilde{T}_c$ as a meaningful quantity to characterize the local magnetic behavior of the simulated graded samples, which is also in agreement with renormalization group theory predictions on simple inhomogeneous ferromagnetic systems [37]. To continue the quantitative analysis of our simulation results, we considered two different approaches to determine the numerical $\tilde{T}_c(z)$ profiles. The first one consisted of using a polynomial fit of the layer-wise χ vs. T curves for every given z and then selecting the temperature at which the maximum occurred to define $\tilde{T}_c^{\chi} = T[\chi(z)^{\max}]$. The second approach consisted of estimating $\tilde{T}_c^M$ by means of the fitting parameter according to Eq. (7).

Figure 3(c) shows a comparison between the two approaches considered for obtaining $\tilde{T}_c(z)$. As previously mentioned, $\tilde{T}_c^{\chi}(z)$ (depicted as red squares) is obtained as the temperature at which the maximum of each $\chi(z)$ curve occurs, whereas $\tilde{T}_c^M(z)$ (depicted as open symbols) is obtained as the fitting parameter of Eq. (7) for every local $M(z)$ curve.

[2]The shape parameter s was computed as the mean value of the best-fitted layer-specific s parameters at the inner portion of the sample. We found $\langle s \rangle = 1.757$ to be within the range of reported values for experimental systems, and it was kept fixed throughout further analysis [50]. Using a single set of values for p and s is consistent with the underlying assumption that local $M(T)$ data for similar but different J_z should fall into the same universality class, exhibiting the same critical exponents and thus the same shape [21].

Figure 3(c) shows that both distributions evolve predominantly in a linear fashion with z, at least for the interior of the structure away from the surfaces. Near both surfaces, we observe that $\tilde{T}_c(z)$ values exhibit a noticeable drop. This effect is caused by the lack of nearest neighbors at the surfaces, which reduces the total exchange coupling field, leading to a reduced $\tilde{T}_c$ at and near both surfaces. From this figure, it is evident that both distributions follow each other very well except at the high J_z portion of the sample, where the $\tilde{T}_c^{\chi}(z)$ data seem noisier than the $\tilde{T}_c^M(z)$ profile. In fact, because of the mapping of the temperature-dependent ferromagnetic state onto the depth-dependent profile, it is also near this portion of the sample where the largest local fluctuations occur. Hence, around the high J_z portion of the sample is where the system starts to order as a whole, at the very point where the sample exhibits its largest $\tilde{T}_c$ value.

For our further analysis and discussion, we decided to use the $\tilde{T}_c^M(z)$ data for two reasons: (i) the $\tilde{T}_c^M(z)$ distribution is derived from local magnetization data, using all available information for the entire range of simulated temperatures and not just the ones near each $\tilde{T}_c(z)$ [as $\tilde{T}_c^{\chi}(z)$]. Therefore, it allows for a more robust and reliable $\tilde{T}_c$ analysis, which is actually corroborated by Fig. 3(c), where the red data points are indeed noisier, at least near the high $\tilde{T}_c(z)$ portion of the sample. (ii) Besides simply simulating the thermodynamic properties of graded materials, we also aim in this study at determining a generally applicable predictive formulation that can describe the spatial distribution of the ferromagnetic state at any given temperature in any graded material. This can be done better utilizing $\tilde{T}_c^M$ because all temperature data actually contribute to its determination. For both these reasons, it is more sensible to use the layer-specific magnetization data and apply Eq. (7) to determine the $\tilde{T}_c^M(z)$ profiles.

C. Resulting $\tilde{T}_c$ profiles

Before further advancing the discussion of our results, it is useful to clearly distinguish between two fundamentally different finite-size effects in our simulated systems. Firstly, there are unintended finite size effects due to the finiteness of the lateral dimension of the sample, which are partially suppressed by utilizing PBC within the x-y plane. These lateral finite-size effects are inherent to all MC simulations and are explicitly verified and discussed in the Appendix. The other

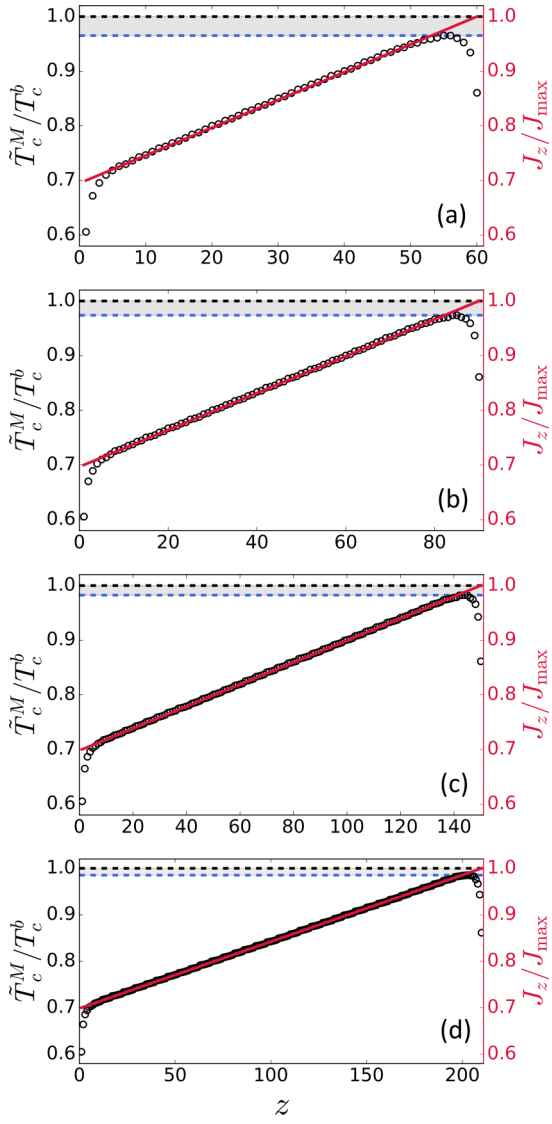

FIG. 4. Simulation extracted layer-dependent $\tilde{T}_c^M/T_c^b$ profiles (open symbols) in comparison to the corresponding exchange constant profiles (solid red lines) for (a) $t = 60$, (b) $t = 90$, (c) $t = 150$, (d) $t = 210$. The black and blue dashed lines represent the normalized global T_c of the uniform and graded samples for every given t value, respectively.

finite size effect that also occurs in real experimental samples and is thus far more interesting is caused by the finite thickness of the utilized film geometry. Thus, for the purpose of testing the t dependence of the $\tilde{T}_c^M(z)$ profiles, we performed simulations for samples with varying t values ranging from 60 to 210 for $L = 20$. Figure 4 shows the resulting $\tilde{T}_c^M/T_c^b$ profiles (open symbols) compared to the linear-gradient J_z of Eq. (1) (red solid lines) for (a) $t = 60$, (b) $t = 90$, (c) $t = 150$, and (d) $t = 210$, with T_c^b being the T_c of a three-dimensional uniform bulk system with $J_{\max}$. From this figure, it can be deduced that already a simple and purely local J_z picture is fairly accurate to characterize the $\tilde{T}_c^M(z)$ profiles, except for the near surface areas on the top and bottom of the graded film. More importantly, it can be seen from the figure that as t gets larger, the "surface error regions" becomes relatively

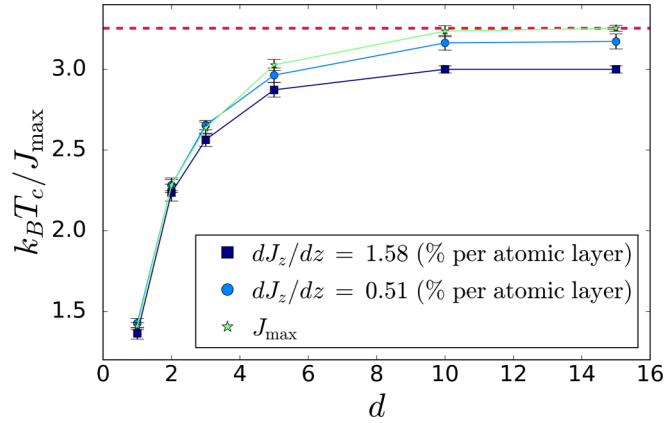

FIG. 5. Finite-thickness dependence of the global T_c for a uniform sample with $J_{\max}$, and two graded samples exhibiting two different gradient values, whose quantities are defined in units of J_z reduction (in percent of $J_{\max}$) per layer. The symbols are our simulation results and the lines are a guide to the eye. The red dashed line represents the T_c^b of a uniform three-dimensional system with $J_{\max}$.

smaller, showing that there is a noticeable t-dependence of the $\tilde{T}_c^M(z)$ profiles. This surface behavior is triggered by the fact that some of the nearest neighbors are missing at the surface because of the FBC imposed along the z axis, which reduces the total exchange coupling energy for the surface layers. Thus, less thermal energy will be required to break the magnetic order at surfaces, which leads to reduced $\tilde{T}_c$ values at and near both surfaces. This behavior propagates a few layers deep into the interior of the sample until, at some point, the exchange field is balanced, causing $\tilde{T}_c^M(z)$ to mimic the local exchange strength J profile exactly.

The global T_c of the graded systems investigated here is equivalent to the maximum of $\tilde{T}_c^M(z)$ since, at this temperature, the graded sample starts to order ferromagnetically. In Fig. 4, we observe that the larger t is, the closer is the global T_c to T_c^b, which we have visualized by means of blue and black dashed lines that approach each other as we increase t. This increase of the global T_c is related to the lowering of the gradient term $dJ_z/dz = (J_{\max} - J_{\min})/(t-1)$ of Eq. (1), which is the rate at which J_z varies along z. Thus, whenever we increase t, there will be more layers with J_z values close to $J_{\max}$ at the high J end of the sample. This leads to an increase in the global T_c of the whole system, since this is a depth-averaged related quantity.

To explain the observed global T_c effect that occurs at the high J end of the sample, Fig. 5 shows the finite-thickness effect on the global T_c, computed for three $L\times L\times d$ sized samples. We considered one sample featuring a uniform $J_{\max}$ distribution (green stars) and two graded samples featuring J_z profiles exhibiting a 30% absolute reduction in the exchange strength along the z axis, albeit each one having different gradient values corresponding to $dJ_z/dz = 1.58\%$ (dark blue squares) and $dJ_z/dz = 0.51\%$ (light blue circles), whose quantities are defined in units of J_z reduction (in percent of $J_{\max}$) per layer. Let us first turn the discussion to the uniform case, from which one can see that a certain number of layers is needed to come close to the bulk value T_c^b, following

a film thickness scaling law [52–56]. Now, when analyzing the curves for the graded samples, it can be seen that they exhibit the same saturation type behavior of the uniform case, approaching the bulklike T_c as d increases. However, given that now the exchange constant is going down with d, new layers are less and less able to support the buildup of the ferromagnetic state at the global T_c, so that the thickness-dependent T_c saturates earlier and at a lower value if compared to the uniform $J_{\max}$ case. Furthermore, Fig. 5 also shows that a steeper gradient leads to a lower saturation value of the global T_c, which is exactly the type of behavior that we observe in Fig. 4 for different simulated gradients. Thus, all aspects of the $\tilde{T}_c^M(z)$ profiles we observe in Fig. 4 can be well understood. The here discussed global T_c effect also explains the behavior observed in Fig. 2(a), where the T_c values of the uniform sample with $J_{\max}$ (blue triangles) and the graded sample (green squares) are not equal. It is also important to mention that we find the local behavior to be very accurate, even though the ratio of the intra- to the interlayer exchange coupling strength is close to unity for our simulated structures in contrast to previous studies that focused primarily on weakly interacting layer systems [28].

D. Predictive formulation

Given the fact that the pure local J picture is already reasonably close to predicting the local magnetic behavior and associated $\tilde{T}_c^M$, we now aim at developing a predictive model for $M(z, T)$, whose only input is the J_z profile and which would not rely on doing full scale modeling or experiments. It is sensible to consider that, in order to achieve a very precise $M(z, T)$ description, it will be crucial to have a very precise $\tilde{T}_c^M(z)$ prediction from a given J_z profile. Hereby, Fig. 4 shows us that a fully local picture is not completely accurate in predicting the local $\tilde{T}_c^M$ at and near the surfaces, where the J_z change is largest, namely abrupt, so that nonlocal effects occur most strongly. Also, Fig. 5 shows us that the global T_c of graded samples depends on the buildup of an effective volume that contributes to the aggregation of the ferromagnetic state. So, one ought to consider a weighted average of J_z rather than a purely local picture and also take into account the number of nearest neighbors, which each spin actually has. Here, we assume that the relevance of more distant layers decays exponentially with ζ being the relevant decay length. Under these assumptions the predicted local Curie temperature profile $\tilde{T}_c^p(z)$ (where the superscript p stands for 'predictive') based solely on the J_z profile is

$$\tilde{T}_c^p(z) = T_c^b \frac{\sum_{z'=1}^{t} \frac{N^{z'}}{12} J_{z'} \exp\left(-\frac{|z-z'|}{\zeta}\right)}{J_{\max} \sum_{z'=1}^{t} \exp\left(-\frac{|z-z'|}{\zeta}\right)}, \tag{8}$$

where $N^{z'}$ is the number of nearest neighbors that a spin in the z' layer has. The 12 in the numerator corresponds to the coordination number of the fcc crystal lattice. The summations are taken over all t layers, considering only layers that are present in the actual physical structure.

Figure 6(a) shows $\tilde{T}_c^M(z)$ (open symbols) along with $\tilde{T}_c^p(z)$ for three arbitrary ζ values (dark blue, light blue, and light green solid lines, respectively), given in units of layers. It is observed from this figure that a high value of $\zeta = 20$ (light green) approaches a purely collective nature, with the relevance of nonlocal properties being very significant over large length scales. In the extreme case of even higher ζ values, $\tilde{T}_c(z)$ would tend to converge to the $\tilde{T}_c$ of a uniform sample with an average constant J. Therefore, the $\zeta = 20$ curve does not properly describe the simulated $\tilde{T}_c^M$ data because the real thermodynamic magnetic behavior of a graded sample is far more local than this value assumes it to be. For the low $\zeta = 0.2$ value (dark blue) in Fig. 6(a), the observed effect is just the opposite, basically recreating a purely local description, which evidently cannot describe the behavior at and near the surfaces, where the J_z change is very abrupt. Instead, we can see in Fig. 6(a) that for an intermediate yet still low value $\zeta = 2$, the obtained $\tilde{T}_c^p$ curve describes the $\tilde{T}_c^M(z)$ profile quite well.

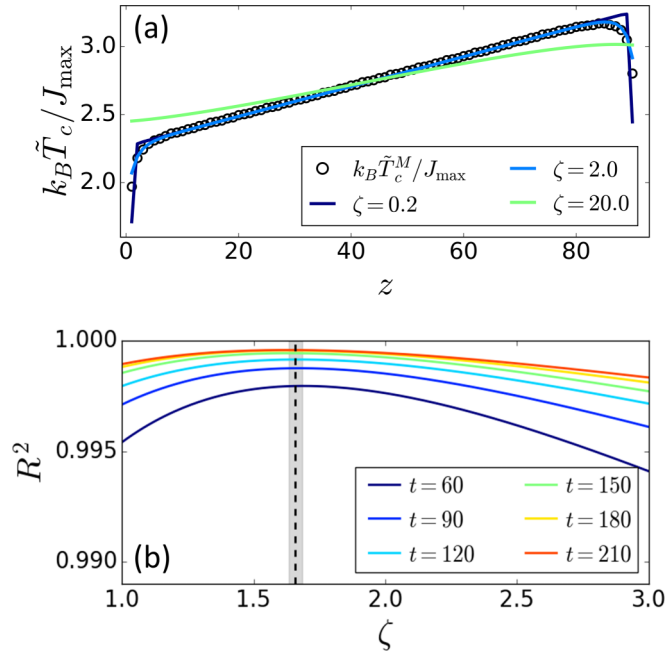

FIG. 6. (a) Simulation extracted $\tilde{T}_c^M(z)$ profile for $t = 90$ as open symbols, in comparison to the obtained $\tilde{T}_c^p$ profile according to Eq. (8) for several values of ζ as solid lines. (b) R^2 vs ζ for Eq. (8) to reproduce the simulation extracted $\tilde{T}_c^M(z)$ profiles for different t. The shaded region is a superposition of all standard deviation regions, while the vertical dashed line represents the mean value of the optimum ζ, i.e., $\zeta^* = 1.66 \pm 0.03$.

To determine the most suitable ζ value we computed $\tilde{T}_c^p(z)$ for values of ζ in the range of 1–3 and compared the results quantitatively with our simulated $\tilde{T}_c^M(z)$ data by determining the coefficient of determination R^2. Figure 6(b) displays the resulting R^2 values and shows that there is an optimum ζ value for any given sample thickness t we computed. Furthermore, we see that the resulting R^2 values are very close to 1 and more importantly, that the optimum ζ value (ζ^*) is essentially t-independent, since all the R^2 curves exhibit a maximum around the same ζ. The shaded region in Fig. 6(b) contains all the ζ^* values, and the black dashed line represents the mean of all determined $\zeta^* = 1.66 \pm 0.03$ with the error representing the standard deviation of the mean value of the resulting ζ^* for all t. It is relevant to point out that, as ζ^* is dominated by the

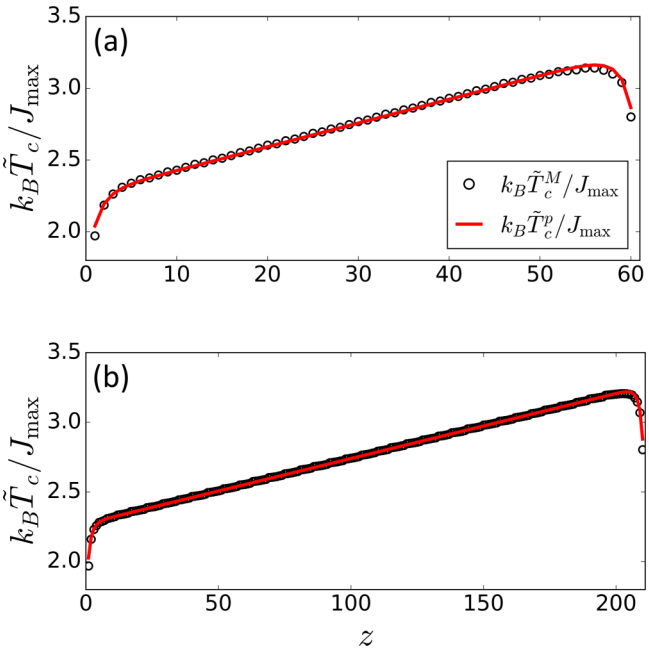

FIG. 7. $\tilde{T}_c$ profiles for (a) $t = 60$, (b) $t = 210$; open symbols represent the simulation extracted $\tilde{T}_c^M(z)$ data, whereas the solid lines show the profiles obtained via Eq. (8) using only a single value $\zeta^* = 1.66$ and the exchange constant profiles according to Eq. (1).

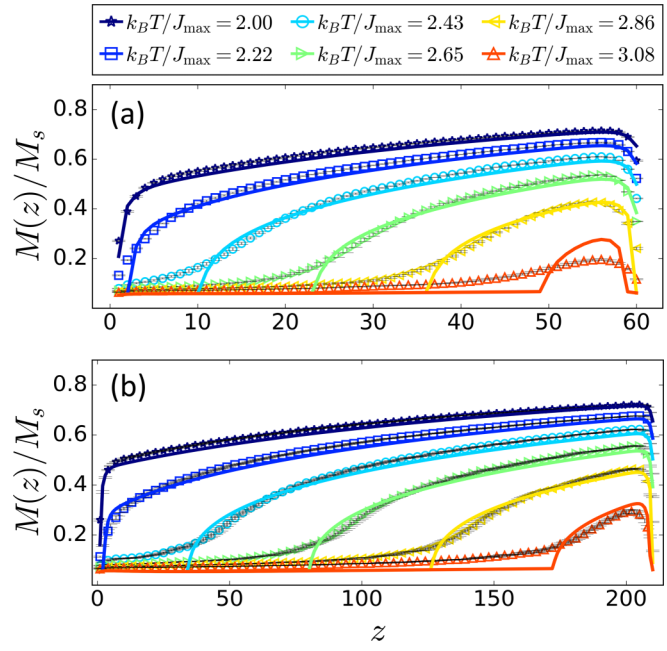

FIG. 8. Layer-dependent magnetization profiles for several constant temperatures. The open symbols represent the simulated data whereas the solid lines represent the predicted profiles, by obtaining the local temperature-dependent magnetization curves using our formulation, with $s = 1.757$, $p = 5/2$, together with the computed $\tilde{T}_c^p$ distribution, for (a) $t = 60$ and (b) $t = 210$. It is important to mention that in (b), only a third of all the simulated data points are shown to avoid an overlapping of the symbols.

behavior at the surfaces, where changes in the exchange field are abrupt, the ζ^* values for different t are very similar, because the surface effects are similar in nature for all t, regardless of how steep or shallow the J_z distribution is in the interior of the graded sample. Most relevantly, though, the t-independent and small value of $\zeta^* = 1.66$ confirms the dominance of the local thermodynamic behavior in our simulations. As such, the here determined ζ^* value is consistent with prior observations on metallic band ferromagnets, for which this length scale was reported to be of the order of 1–2 nm [21].

Figure 7 now shows $\tilde{T}_c^M(z)$ (open symbols) along with $\tilde{T}_c^p$ (red solid lines) for the two limiting cases of our simulations, namely (a) $t = 60$ and (b) $t = 210$ using Eq. (8) with fixed $\zeta^* = 1.66$ and the predefined J_z profiles. The plots confirm that our general description can predict the $\tilde{T}_c^M(z)$ profiles very accurately regardless of t. From this, we can assert that our formulation describes the buildup of the ferromagnetically ordered portion of the sample very well. This alone, however, does not guarantee that the overall resulting temperature dependent magnetization profiles are well described, because $\tilde{T}_c^p$ only describes the temperature at which ferromagnetism occurs but not its temperature evolution in the ferromagnetic state. Thus, we have to investigate the predictive power and accuracy for actual magnetization profiles next.

For this we utilize the calculated $\tilde{T}_c^p(z)$ profiles that are predicted from the J_z profile alone in conjunction with the Kuz'min formula [Eq. (7)] and thus make a prediction of $M(z, T)$ for any profile and at any temperature. Figure 8 shows $M(z, T)$ profiles for a few selected temperatures, for the two limiting cases in our simulations (a) $t = 60$ and (b) $t = 210$. In this figure, the simulation data points are depicted as open symbols, whereas the predicted profiles are shown as solid lines. In Figs. 8(a) and 8(b), we find that the simulated data points are very well described by our formulation in almost the entirety of the graded samples, even at and near both surfaces, especially for low and intermediate temperatures. Nonetheless, there are visible deviations in between predicted and simulated data for the largest temperature (orange $k_BT/J_{\max} = 3.08$ curves) at the high J portion of the samples, while said deviations are found to be less significant for the thicker sample. This comes from the fact that the $\tilde{T}_c^p(z)$ profile of the $t = 60$ sample exhibits slightly overestimated values on the high z side, which are visible in Fig. 7(a), causing slightly larger predicted M values in the high J portion of the graded sample near its global T_c.

Figure 8 also shows that in these graded samples, one encounters a quasi phase-boundary separating ordered from disordered magnetic regions within the sample, in which the temperature-dependent ferromagnetic state is mapped onto a depth-dependent profile, as was predicted in prior work [18–21]. We can also see from Fig. 8 that this quasi phase-boundary is not infinitely sharp but has a certain extension, due to the fact that ferromagnetically ordered layers induce via interlayer exchange coupling a nonvanishing magnetization into adjacent paramagnetic layers. Our predictive $\tilde{T}_c^p(z)$ profile description cannot reproduce this finite transition region, so that we observe numerical deviations also in these portions of the $M(z, T)$ profiles. However, the induced magnetization falls off exponentially in the paramagnetic segments, so that the numerical discrepancies in between the simulated and

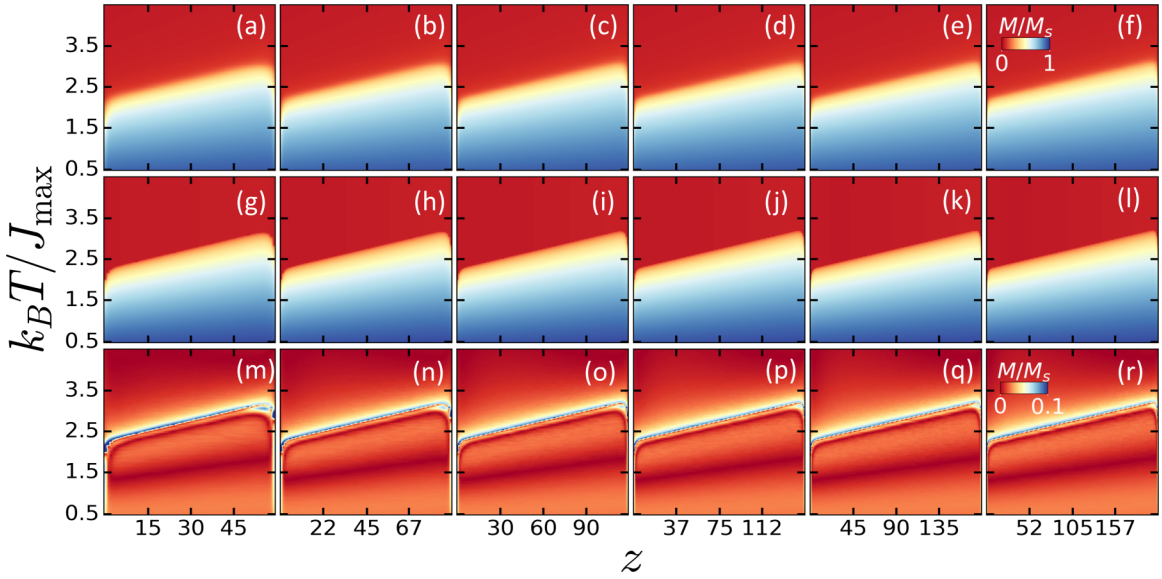

FIG. 9. Color-coded maps of layer and temperature dependent magnetization data for different film thickness t; the figure shows the MC simulated data [(a)–(f)], the predicted local magnetization data using the computed $\tilde{T}_c^p$ profiles [(g)–(l)], and the absolute difference between both sets of data [(m)–(r)]. The color bar in (f) applies to figures (a)–(l), whereas the color bar in (r) is valid for (m)–(r). Each column represents the maps for one specific film thickness t, namely from left to right $t = 60$, 90, 120, 150, 180, and 210.

predicted magnetization profiles are rather modest. So, while our estimates for the local $\tilde{T}_c$ have included some nonlocal averaging to generate a predicted $\tilde{T}_c(z)$ profile, we are using this profile subsequently in a purely local approach, leading to a sharp interface in the $M(z, T)$ profiles, which does not fully reflect the nature of the coupled systems. Regardless of these rather small deviations, the formulation presented in this work substantially supports the fact that the thermodynamic magnetic behavior of exchange graded ferromagnets can be well described in terms of local material properties [21].

To substantiate the reliability of the predictive description we derived here, Fig. 9 shows color-coded maps for all our simulation results [Figs. 9(a)–9(f)], the corresponding analytic $M(z, T)$ profiles [Figs. 9(g)–9(l)], and the absolute difference between both these maps [Figs. 9(m)–9(r)]. Hereby, every column in this figure represents a given t value. All Figs. 9(a) to 9(l) show strongly (blue) and weakly (red) magnetized regions at low and high temperatures, being separated by a continuous transition (white region) at intermediate temperatures. The limit between the white and red regions represents the quasi phase-boundary that emerges, which exhibits a z-dependent transition temperature due to the depth-dependent J_z profile. When comparing Figs. 9(a)–9(f) with Figs. 9(g)–9(l), it can be seen that both data sets are strikingly similar in all cases. Upon closer inspection, however, one can see that the simulated data exhibit a slightly broadened transition from strongly to weakly ordered regions, whereas the predicted data show a more abrupt transition for all z, as discussed in conjunction with Fig. 8. From the differences in between both data sets displayed in Figs. 9(m)–9(r), it can be seen that our predictive description performs remarkably well in the entire range of simulated T and z, with absolute differences smaller than 2% of M_s almost everywhere, except for slightly larger deviations in the immediate vicinity of the quasi phase-boundary, because our local $M(z, T)$ predictions are inherently limited here. More importantly, there is no relevant t dependence of the error results, which implies that our approach should work (with its existing limits) for all kinds of gradient structures, given that the absolute errors are virtually replicated in all cases and thus are not gradient specific. It should also be mentioned that Figs. 8 and 9 also utilize the quantity k, which was defined in Eq. (7) as the remaining "paramagnetic magnetization" above each $\tilde{T}_c$. Hereby, it is important to recall that k is related to finite-size effects in MC simulations (see Appendix) and accordingly not a limit of our predictive approach. Figure 9 also shows that a z layer at $T > \tilde{T}_c$ is not significantly magnetized by an adjacent z layer at $T < \tilde{T}_c$, so that each z layer is found to exhibit a "unique and separate" thermodynamic behavior, which is characterized by layer-specific values of $\tilde{T}_c$. The reason for this is that the interlayer exchange cannot compensate for the high free energy cost to substantially magnetize a paramagnetic layer [21]. Correspondingly, the interlayer coupling does not lead to a large spatial spread of the phase transition in the simulated materials despite its overall very significant strength.

IV. CONCLUSIONS

This work represents the first analysis of magnetization profiles in exchange graded materials based on MC simulations using a classical Heisenberg model with nearest neighbor exchange interactions, with which we have corroborated prior experimental and mean-field calculation findings. We have consequently verified, by using this more accurate type of calculation, that the dominance of local behavior over the collective nature of thermodynamic properties in exchange graded materials exists down to very short length scales. After assessing the outstanding qualitative agreement with available experimental data, we could assert that the local description is indeed fairly precise to characterize the magnetic behavior

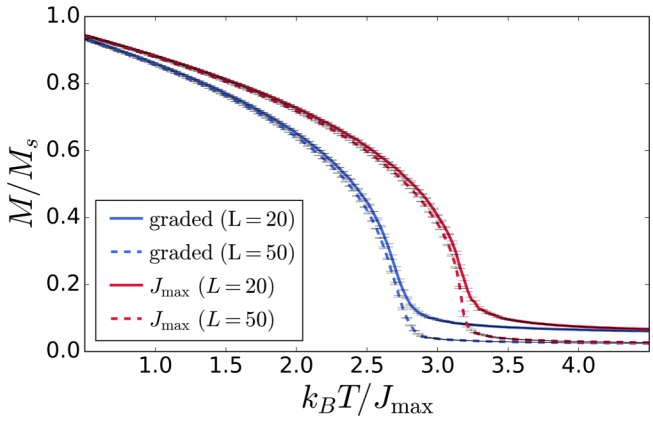

FIG. 10. Dependence of the magnetization on the lateral dimension of the system for the uniform $J_{\max}$ sample together with the local data of the $z = 30$ layer of the graded sample. Solid lines represent magnetization data obtained for a system size of $L = 20$ and $t = 60$, whereas dashed lines represent magnetization data for a system size of $L = 50$ and $t = 60$.

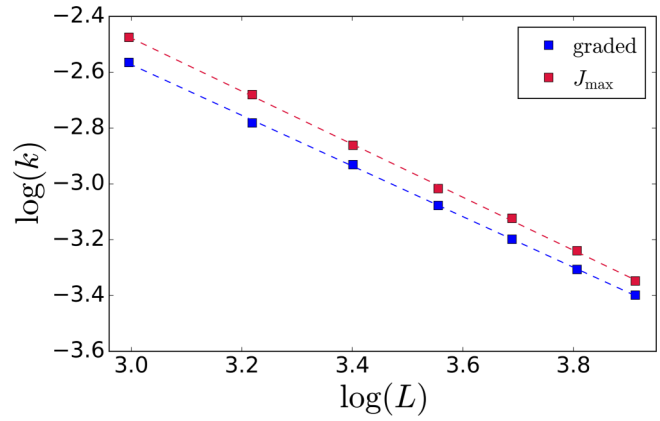

FIG. 11. L-dependence of the k parameter used to account for finite-size effects above $\tilde{T}_c$ for a uniform $J_{\max}$ system and the $z = 30$ layer of the graded sample. The dashed lines are intended as a guide to the eye.

of the simulated materials. Moreover, to continue our endeavor, based upon simulation results, we have developed a predictive description to compute a refined local $\tilde{T}_c$ profile that incorporated nonlocal thermodynamic aspects and which allowed us to achieve a predictive closed-form derivation of temperature-dependent ferromagnetic states at any given temperature, based on the geometry of exchange strength J profiles alone. The derivation of this predictive description also verified that nonlocal nonuniformities are truly significant only over very short length scales. This observation also serves as an indicator for the inherent spatial localization limit in the system, which is in very good agreement with previous experimental estimates. The goal of the predictive description that we derived here is not only to bypass experiments but also the need for MC calculations, which are very time consuming. With our closed-form description, it is now possible to know beforehand which J_z distribution might produce the desired thermodynamic behavior and associated functionality. In this regard, it would be very interesting, for instance, to study more complex exchange profiles, as well as more complex spatial gradients other than only a one-dimensional axial variation, which could then be corroborated by other theoretical approaches and experiments.

ACKNOWLEDGMENTS

J.S.S.G. and J.D.A.C. acknowledge financial support by MINCIENCIAS under the program Jóvenes Investigadores e Innovadores 2018 (Grant No. 812). Work at nanoGUNE acknowledges financial support by the Spanish Ministry of Science and Innovation under the Maria de Maeztu Units of Excellence Program (MDM-2016-0618) and Project No. RTI2018-094881-B-100 (MICIU/Feder).

APPENDIX

We have explicitly verified the finite-size effects, associated with the finiteness of the lateral dimension of the system, i.e., finite L values according to Fig. 1, for individual layers of the graded sample, which behave as the typical finite-size effects on averaged $M(T)$ data of uniform bulk systems. It is important to bear in mind that the choice of a given L relies on the computational time required to obtain dependable simulation results, which increases significantly with size. Therefore, one must assure that the system size is sufficiently large to obtain dependable magnetic information while not requiring a prohibitively large running time. Hereby, it is important to mention that even when the lateral extent of the here explored systems is smaller than their thickness, it does not impact our general conclusions, given that the thickness of individual segments that undergo a quasiphase transition at a given temperature is actually limited to very few layers. Correspondingly, the most relevant thermodynamic behavior is dominated by an effective thin film segment that is substantially thinner than its lateral sample size, even in the case of the smallest L that we utilized.

For the explicit verification of the lateral finite-size effects, we selected the $z = 30$ layer of a graded sample featuring the linear-gradient magnetic exchange profile of Eq. (1) with $J_{\max} - J_{\min} = 0.3$, $t = 60$, and L ranging from 20 up to 50 in steps of $\Delta L = 5$. Then, we compared the $M(T)$ data of the chosen individual layer of the graded sample with that of the three-dimensional uniform bulk system with $J_{\max}$ for the two limiting L values in our simulations ($L = 20$ and $L = 50$).

Figure 10 shows the $M(T)$ data for the uniform $J_{\max}$ sample (red lines) and the $z = 30$ layer of the graded sample (blue lines) for $L = 20$ and $L = 50$ (solid and dashed lines, respectively). From Fig. 10, it can be unambiguously seen that the phase transition is always clearly identifiable, while the transition temperature itself is only modestly impacted by L. This rather modest L dependence of T_c can be explained from the fact that we are computing the magnetization as the absolute value of the spin projections [Eq. (3)]. Thus, upon reducing L, more and more long-range fluctuations are excluded from the actual simulated system, so that the $|M|$ value for any given T modestly increases, as does the perceived T_c. Moreover, it should be noted that, away from the global T_c and due to its rather substantial thickness, the graded film is representative

more of a three-dimensional ferromagnetic system. Most importantly though, Fig. 10 shows that the behavior is essentially the same for the individual layer of the graded and the uniform film, albeit the graded film has a lower T_c, because for the layer we consider here the local J is very relevantly reduced.

Figure 10 also shows for both graded and uniform samples that even when T is significantly larger than T_c, there remains a so-called "paramagnetic magnetization," i.e., a small magnetization above T_c that has not completely averaged to zero [57,58]. Instead, a value of δM is obtained, which depends on both the size of the system and the "time" of the simulation run (measured in MCS). However, we cannot make δM arbitrarily small by increasing the simulation "time". This can be partially suppressed by using finite-size scaling theories; however, such a discussion is not within the scope of our study.

We introduce the k parameter in Eq. (7) to explicitly verify these finite-size effects above $\tilde{T}_c$, while obtaining a complete description for the whole simulated temperature range. Based on our results, we can assert that this k parameter is not unique to graded materials but would have to be used for any analytical data fit of a Kuz'min type formula to analyze any $M(T)$ resulting from MC simulation data. For instance, Fig. 11 shows the L-dependence of the k parameter fitted for the uniform sample and the $z = 30$ layer of the graded system, plotted on a logarithmic scale. From this figure, it can be seen that $k \propto 1/\sqrt{N}$, with $N = L{\times}L{\times}t$, following the standard behavior for this parameter [58], whereas the vertical difference between the two lines comes from the fact that both uniform and graded samples were simulated under the same temperature range. Hence, the farther we are either from T_c^b or $\tilde{T}_c(z = 30)$, the lower the k parameter is [58].

[1] E. F. Kneller and R. Hawig, IEEE Trans. Magn. **27**, 3588 (1991).
[2] E. E. Fullerton, J. S. Jiang, M. Grimsditch, C. H. Sowers, and S. D. Bader, Phys. Rev. B **58**, 12193 (1998).
[3] E. E. Fullerton, J. S. Jiang, and S. D. Bader, J. Magn. Magn. Mater. **200**, 392 (1999).
[4] R. H. Victora and X. Shen, IEEE Trans. Magn. **41**, 2828 (2005).
[5] E. E. Fullerton, D. T. Margulies, N. Supper, H. Do, M. Schabes, A. Berger, and A. Moser, IEEE Trans. Magn. **39**, 639 (2003).
[6] J. U. Thiele, S. Maat, and E. E. Fullerton, Appl. Phys. Lett. **82**, 2859 (2003).
[7] A. Berger, N. Supper, Y. Ikeda, B. Lengsfield, A. Moser, and E. E. Fullerton, Appl. Phys. Lett. **93**, 122502 (2008).
[8] D. Suess, Appl. Phys. Lett. **89**, 113105 (2006).
[9] G. T. Zimanyi, J. Appl. Phys. **103**, 07F543 (2008).
[10] D. Suess, J. Lee, J. Fidler, and T. Schrefl, J. Magn. Magn. Mater. **321**, 545 (2009).
[11] B. J. Kirby, J. E. Davies, K. Liu, S. M. Watson, G. T. Zimanyi, R. D. Shull, P. A. Kienzle, and J. A. Borchers, Phys. Rev. B **81**, 100405(R) (2010).
[12] R. K. Dumas, Y. Fang, B. J. Kirby, C. Zha, V. Bonanni, J. Nogués, and J. Åkerman, Phys. Rev. B **84**, 054434 (2011).
[13] J. Zhang, Z. Sun, J. Sun, S. Kang, S. Yu, G. Han, S. Yan, L. Mei, and D. Li, Appl. Phys. Lett. **102**, 152407 (2013).
[14] C. L. Zha, R. K. Dumas, Y. Y. Fang, V. Bonanni, and J. Nogús, Appl. Phys. Lett. **97**, 182504 (2010).
[15] S. M. Mohseni, R. K. Dumas, Y. Fang, J. W. Lau, S. R. Sani, J. Persson, and J. Akerman, Phys. Rev. B **84**, 174432 (2011).
[16] M. Marcellini, M. Pärnaste, B. Hjörvarsson, and M. Wolff, Phys. Rev. B **79**, 144426 (2009).
[17] C. Le Graët, T. R. Charlton, M. McLaren, M. Loving, S. A. Morley, C. J. Kinane, R. M. D. Brydson, L. H. Lewis, S. Langridge, and C. H. Marrows, APL Mater. **3**, 041802 (2015).
[18] B. J. Kirby, H. F. Belliveau, D. D. Belyea, P. A. Kienzle, A. J. Grutter, P. Riego, A. Berger, and C. W. Miller, Phys. Rev. Lett. **116**, 047203 (2016).
[19] L. Fallarino, B. J. Kirby, M. Pancaldi, P. Riego, A. L. Balk, C. W. Miller, P. Vavassori, and A. Berger, Phys. Rev. B **95**, 134445 (2017).
[20] L. Fallarino, P. Riego, B. Kirby, C. Miller, and A. Berger, Materials **11**, 251 (2018).
[21] B. J. Kirby, L. Fallarino, P. Riego, B. B. Maranville, C. W. Miller, and A. Berger, Phys. Rev. B **98**, 064404 (2018).
[22] K. Schwarz, P. Mohn, P. Blaha, and J. Kübler, J. Phys. F: Met. Phys **14**, 2659 (1984).
[23] P. W. Anderson, Phys. Rev. **124**, 41 (1961).
[24] P. Mohn and K. Schwarz, J. Phys.: Condens. Matter **5**, 5099 (1993).
[25] J. B. Staunton, S. S. Razee, M. F. Ling, D. D. Johnson, and F. J. Pinski, J. Phys. D.: Appl. Phys. **31**, 2355 (1998).
[26] O. Idigoras, U. Palomares, A. K. Suszka, L. Fallarino, and A. Berger, Appl. Phys. Lett. **103**, 102410 (2013).
[27] A. F. Kravets, A. N. Timoshevskii, B. Z. Yanchitsky, M. A. Bergmann, J. Buhler, S. Andersson, and V. Korenivski, Phys. Rev. B **86**, 214413 (2012).
[28] A. F. Kravets, Y. I. Dzhezherya, A. I. Tovstolytkin, I. M. Kozak, A. Gryshchuk, Y. O. Savina, V. A. Pashchenko, S. L. Gnatchenko, B. Koop, and V. Korenivski, Phys. Rev. B **90**, 104427 (2014).
[29] A. F. Kravets, D. M. Polishchuk, Y. I. Dzhezherya, A. I. Tovstolytkin, V. O. Golub, and V. Korenivski, Phys. Rev. B **94**, 064429 (2016).
[30] P. W. Kasteleijn and J. Van Kranendonk, Physica **22**, 317 (1956).
[31] P. R. Weiss, Phys. Rev. **74**, 1493 (1948).
[32] M. E. Lines, Phys. Rev. **133**, A841 (1964).
[33] H. B. Callen, Phys. Rev. **130**, 890 (1963).
[34] P. J. Jensen and K. H. Bennemann, Surf. Sci. Rep. **61**, 129 (2006).
[35] Y. T. Millev and M. A. B. Whitaker, Am. J. Phys. **63**, 1146 (1995).
[36] Y. Millev and M. Fähnle, Phys. Rev. B **51**, 2937 (1995).
[37] U. Krey, Physica B **80**, 231 (1975).
[38] R. F. L. Evans, W. J. Fan, P. Chureemart, T. A. Ostler, M. O. A. Ellis, and R. W. Chantrell, J. Phys.: Condens. Matter **26**, 103202 (2014).
[39] R. F. L. Evans, U. Atxitia, and R. W. Chantrell, Phys. Rev. B **91**, 144425 (2015).

[40] N. D. Mermin and H. Wagner, Phys. Rev. Lett. **17**, 1133 (1966).
[41] N. Leo, S. Holenstein, D. Schildknecht, O. Sendetskyi, H. Luetkens, P. M. Derlet, V. Scagnoli, D. Lançon, J. R. Mardegan, T. Prokscha, A. Suter, Z. Salman, S. Lee, and L. J. Heyderman, Nat. Commun. **9**, 2850 (2018).
[42] J. D. Alzate-Cardona, D. Sabogal-Suárez, O. D. Arbeláez-Echeverri, and E. Restrepo-Parra, Rev. Mex. Fis. **64**, 490 (2018).
[43] J. D. Alzate-Cardona, D. Sabogal-Suárez, R. F. L. Evans, and E. Restrepo-Parra, J. Phys.: Condens. Matter **31**, 95802 (2019).
[44] D. P. Landau and K. Binder, *A Guide to Monte Carlo Simulations in Statistical Physics* (Cambridge University Press, New York, 2009).
[45] D. Hinzke and U. Nowak, Phys. Rev. B **58**, 265 (1998).
[46] R. Kubo, J. Phys. Soc. Japan **12**, 570 (1957).
[47] S. Ramasesha, Proc. Indian Acad. Sci. (Eng. Sci.) **2**, 29 (1979).
[48] W. Xue, G. S. Grest, M. H. Cohen, S. K. Sinha, and C. Soukoulis, Phys. Rev. B **38**, 6868 (1988).
[49] L. H. Bennett, R. D. McMichael, L. J. Swartzendruber, R. D. Shull, and R. E. Watson, J. Magn. Magn. Mater. **104–107**, 1094 (1992).
[50] M. D. Kuz'min, Phys. Rev. Lett. **94**, 107204 (2005).
[51] K. Binder, J. Comput. Phys. **59**, 1 (1985).
[52] P. J. Jensen, H. Dreyssé, and K. H. Bennemann, Surf. Sci. **269-270**, 627 (1992).
[53] L. Szunyogh and L. Udvardi, J. Magn. Magn. Mater.. **198-199**, 537 (1999).
[54] E. Almahmoud, I. Kornev, and L. Bellaiche, Phys. Rev. B **81**, 064105 (2010).
[55] G. A. T. Allan, Phys. Rev. B **1**, 352 (1970).
[56] M. E. Fisher and M. N. Barber, Phys. Rev. Lett. **28**, 1516 (1972).
[57] K. Binder, Phys. Lett. A **30**, 273 (1969).
[58] R. E. Watson, M. Blume, and G. H. Vineyard, Phys. Rev. **181**, 811 (1969).